CHAPTER 4

CERIUM SUBSTITUTED Y-TYPE BARIUM HEXAFERRITE (Co_2-Y); AS A HETEROGENEOUS CATALYST FOR OXIDATION OF STYRENE

4.1 Introduction

The major issue of the selective oxidation of styrene is due to intricate preparation techniques, high costs of catalysts or oxidants, severe conditions, and low conversion efficiency. Recently, hexagonal ferrites have been well-recognized magnetic materials in various application fields. Nanometer-sized ferrite catalyst may enhance its catalytic activity. The $Ba_2Co_2Fe_{12}O_{22}$ ferrites have been studied due to several advantages likewise better thermochemical stability, excellent mechanical hardness, wear and corrosion resistance, higher value of Curie temperature, magnetic recycling, and redox characteristics [(Jotania & Virk, 2012), (Tasca *et al.*, 2012), (Dhakshinamoorthy *et al.*, 2011)].

The cerium-substituted Y-type barium hexaferrite $Ba_{2-x}Ce_xCo_2Fe_{12}O_{22}$ (x = 0.0, 0.1, 0.2, & 0.3) are synthesized using the nitrate-based sol-gel auto combustion method and investigated their catalytic efficiency within the formation of benzaldehyde through oxidizing the styrene. The proposed hexaferrite samples are prepared using the analytical grades of barium nitrate [$Ba(NO_3)_2$], cerium nitrate [$Ce(N0_3)_3.6H_20$], cobalt nitrate [$Co(NO_3)_3.6H_2O$], ferrous nitrate [$Fe(NO_3)_3.9H_2O$] as elemental precursors and citric acid [$C_6H_8O_7 \cdot H_2O$] as a chelating agent or fuel within the process. The selection of cerium as a substituting element is inspired by the earlier studied spinal ferrite $Ce_xCo_{1-x}Fe_2O_4$ system, where the substitution of cerium at the spinal A site results in the formation of CeO_2 as an impurity phase (a known oxidation catalyst) on the catalyst surface, resulting to the enhancement for both the conversion of styrene and selectivity of benzaldehyde up to x = 0.3 [(Tong, Li, Bo, Wang, Hu, & Zhang, 2016)].

The synthesized cerium-substituted Y-type hexaferrite nanoparticles are successfully used as magnetically recoverable and heterogeneous catalysts for styrene oxidation in the presence of trifluoroacetic acid (TFA) as an oxidant. It is observed that the presence of TFA accelerates the oxidation and also contributes to lowering the risk of

handling (explosiveness) during the process at ambient temperature as compared with a widely used oxidant like hydrogen peroxide (H_2O_2). The effects of catalyst amount, reaction temperature & time, solvent, and oxidizing agent required for the entire conversion of styrene to benzaldehyde are also examined with pure Y-type barium hexaferrite (Co_2-Y). The catalytic performance of the Co_2-Y powder is measured for its suitability in the oxidation of styrene using various oxidants. The isolated yield of the benzaldehyde is calculated using column chromatography separation. The effect of cerium substitution on the benzaldehyde selectivity is also analyzed at optimized conditions.

The selective oxidation of styrene is evaluated with styrene (1 Equiv), TFA (1 Equiv), and 20 mg of pure barium hexaferrite powder as a catalyst for a typical procedure. The ingredients are mixed in a reaction tube with 1.5 ml of aqueous methanol: water (3:2) solution as a solvent. The resulting reaction mixture is continuously stirred in a sealed reaction tube as per the desired period and temperature using an oil bath. After completion of the reaction, the mixture is cooled down at room temperature, and the product is extracted through solvent extraction using ethyl-acetate (20 ml) twice. The extracted product is further washed with the water and dried over anhydrous Na_2SO_4. The solvent is evaporated at reduced pressure on a rotary evaporator. The formation of the desired product is confirmed through the thin layer chromatography (TLC) co-spotting method with the standards as a reference. An incurred crude product is purified by silica-gel column chromatography using ethyl acetate/hexane to dilute the mixture. Finally, the obtained solid/liquid product is characterized by ^{1}H and ^{13}C NMR spectroscopy analysis.

4.2 Results and discussion

The XRD pattern of the calcined cerium substituted barium hexaferrite is shown in Fig. 4.1(a). It is confirmed that the single Y-type barium hexaferrite phase is formed after

calcination at 1200°C. Cerium substituted samples show cerium oxide as an impurity phase. The peaks obtained in the XRD pattern for these hexaferrite samples match exactly with the standard JCPDS card no 440206 for $Ba_2Co_2Fe_{12}O_{22}$ and JCPDS card no 750390 for CeO_2 as an impurity phase.

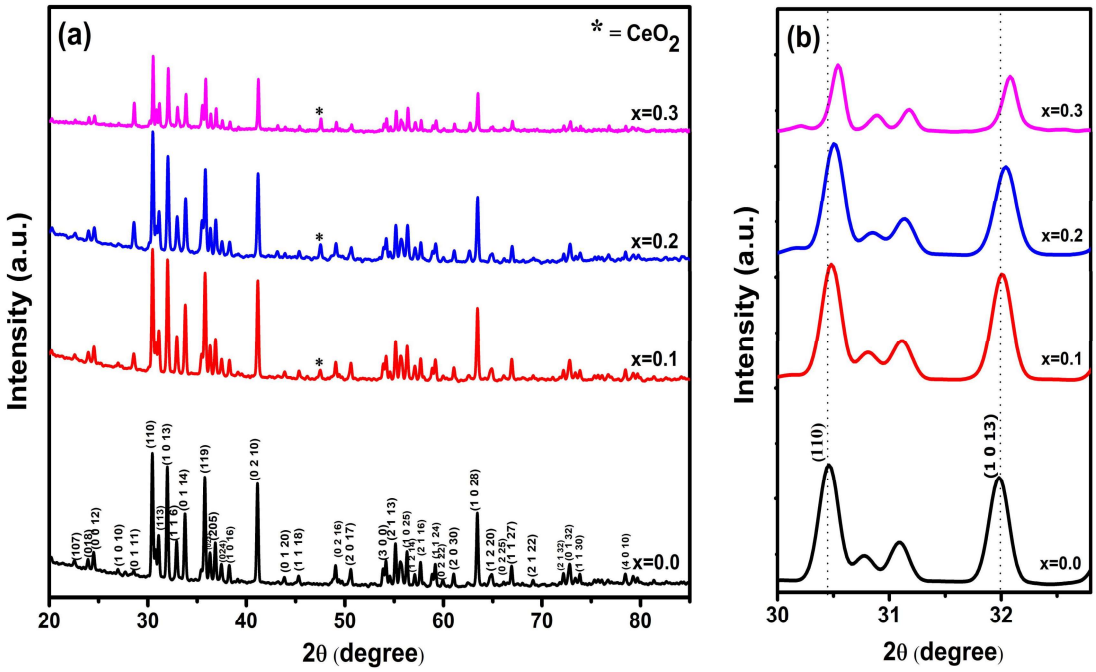

Figure 4.1 (a) XRD patterns of calcined $Ba_{2-x}Ce_xCo_2Fe_{12}O_{22}$ (x = 0.0, 0.1, 0.2, & 0.3) ferrites, (b) Peak shifting of (110) and (1013) peaks.

The structural parameters such as crystallite size, lattice constants (*a* and *c*), *c/a* ratio, unit cell volume, surface area, and X-ray density are calculated and shown in Table 4.1. The X-ray pattern reveals that the Ce^{3+} can be nearly substituted in the composition of $Ba_{2-x}Ce_xCo_2Fe_{12}O_{22}$ ferrite. The peak intensity corresponding to the CeO_2 impurity phase gets stronger with the substitutional amount [(Araz, 2019), (Mosleh *et al.*, 2016)]. It suggests that the limit of solubility of substituted cerium in ferrite is achieved in the composition. A similar dual-phase system in barium hexaferrite with Ce substitution is also observed by Vakil *et al.* [(Vakil *et al.*, 2015)]. A minor reduction in the lattice constant and right-hand

side shifting (Fig. 4.1 (b)) of Bragg peak position corresponding to (110) & (1013) can be detected. It depicts the replacement of the larger ion Ba^{+2} (1.34 Å) with a smaller substituted ion Ce^{+3} (1.034 Å). The crystallite size, as well as the cell volume, also decreases with Ce^{3+} substitution in the ferrites. It can also be found that the addition of cerium also leads to an increase in the surface area. An increase in X-ray density is attributed due to the higher atomic mass of Ce^{+3} in comparison with Ba^{+2}.

Table 4.1 Crystallite size, lattice parameters, *c/a* ratio, cell volume, surface area, and X-ray density of $Ba_{2-x}Ce_xCo_2Fe_{12}O_{22}$ (x = 0.0, 0.1, 0.2, & 0.3) ferrites.

Sample	Crystallite size (nm)	*a* (Å)	*c* (Å)	*(c/a)*	Cell volume ($Å^3$)	Surface area (m^2g^{-1})	X-ray density (g/cm^3)
$Ba_2Co_2Fe_{12}O_{22}$	48.02	5.866	43.562	7.426	1298.194	39	5.428
$Ba_{1.9}Ce_{0.1}Co_2Fe_{12}O_{22}$	47.41	5.866	43.545	7.423	1297.598	43	5.432
$Ba_{1.8}Ce_{0.2}Co_2Fe_{12}O_{22}$	44.58	5.866	43.492	7.414	1296.019	47	5.439
$Ba_{1.7}Ce_{0.3}Co_2Fe_{12}O_{22}$	45.40	5.866	43.476	7.411	1295.580	44	5.443

FTIR is employed to evaluate the chemical bonding present in the as-synthesized samples calcined at 1200°C, as shown in Fig. 4.2. Bands between 400-800 cm^{-1} are the major characteristic bands of the ferrite [(Chaudhari *et al.*, 2013)]. A slight shifting of these characteristic bands towards the higher wavenumber with substitution is due to the decrease in cell volume [(Almessierea *et al.*, 2019)]. Two absorption peaks around 580 cm^{-1} and 400 cm^{-1} are observed in all these samples corresponding to the tetrahedral and octahedral metal ion vibrations, respectively. It is assigned due to the expansion of metal-oxygen bonds. It may be due to Fe-O stretching and attributed to the formation of hexaferrite [(Temuujin *et al.*, 2004)]. The force constant (F) and bond length (L_b) values for the Fe-O bond are calculated and tabulated in Table 4.2.

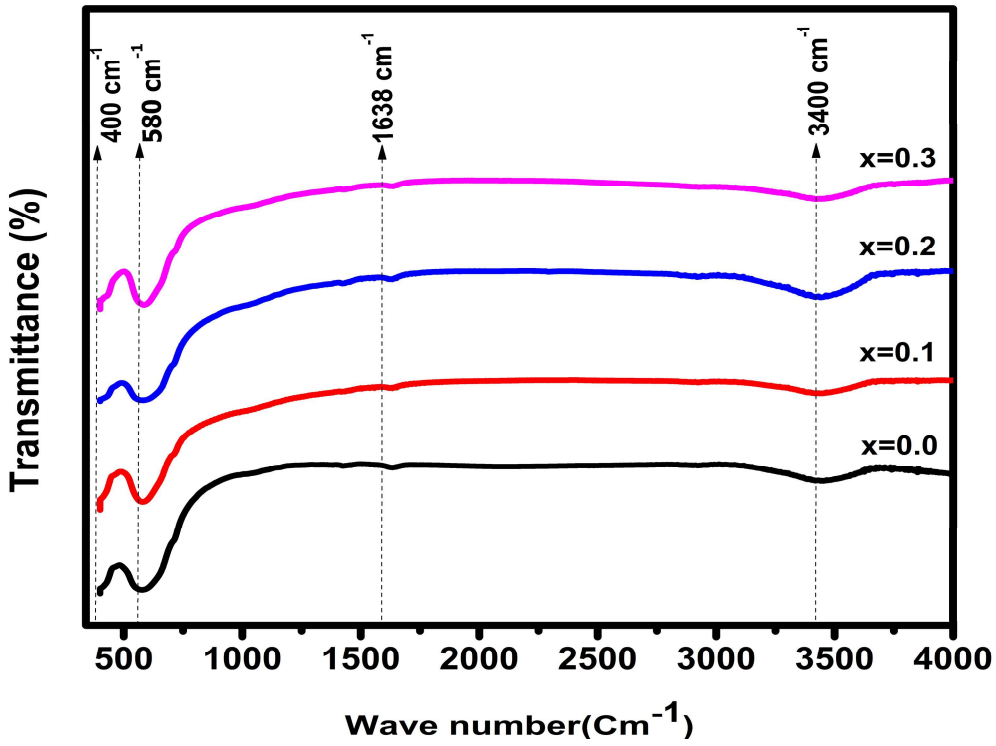

Figure 4.2 FT-IR spectra of calcined $Ba_{2-x}Ce_xCo_2Fe_{12}O_{22}$ (x = 0.0, 0.1, 0.2, & 0.3) ferrite powders.

Table 4.2 Wave number, effective mass, force constant, and bond length of $Ba_{2-x}Ce_xCo_2Fe_{12}O_{22}$ (x = 0.0, 0.1, 0.2, & 0.3) ferrites.

Sample	Wave number (cm^{-1})	Effective mass (10^{-26} kg)	Force constant (N/cm)	Bond length (Fe–O) (Å)
$Ba_2Co_2Fe_{12}O_{22}$	577.57	2.065	2.446	1.908
$Ba_{1.9}Ce_{0.1}Co_2Fe_{12}O_{22}$	580.46	2.065	2.471	1.902
$Ba_{1.8}Ce_{0.2}Co_2Fe_{12}O_{22}$	581.43	2.065	2.479	1.899
$Ba_{1.7}Ce_{0.3}Co_2Fe_{12}O_{22}$	584.80	2.065	2.508	1.892

It is confirmed that the addition of cerium leads to decreasing bond lengths and ensures cell volume contraction, as obtained in the X-ray diffraction pattern. Apart from these characteristic bands, another absorption peak around 1638 cm^{-1} is also found. It can

be correlated to the presence of the stretching and bending modes of H–O–H or N–H band that can be due to the use of ammonia solution to adjust the pH. It is also found to have a broader absorption peak around 3400 cm^{-1} for O–H stretching, which can be attributed to the presence of some moisture in the samples [(Lalegani & Nemati, 2015), (Abbas, Parvatheeswara Rao, *et al.*, 2014)].

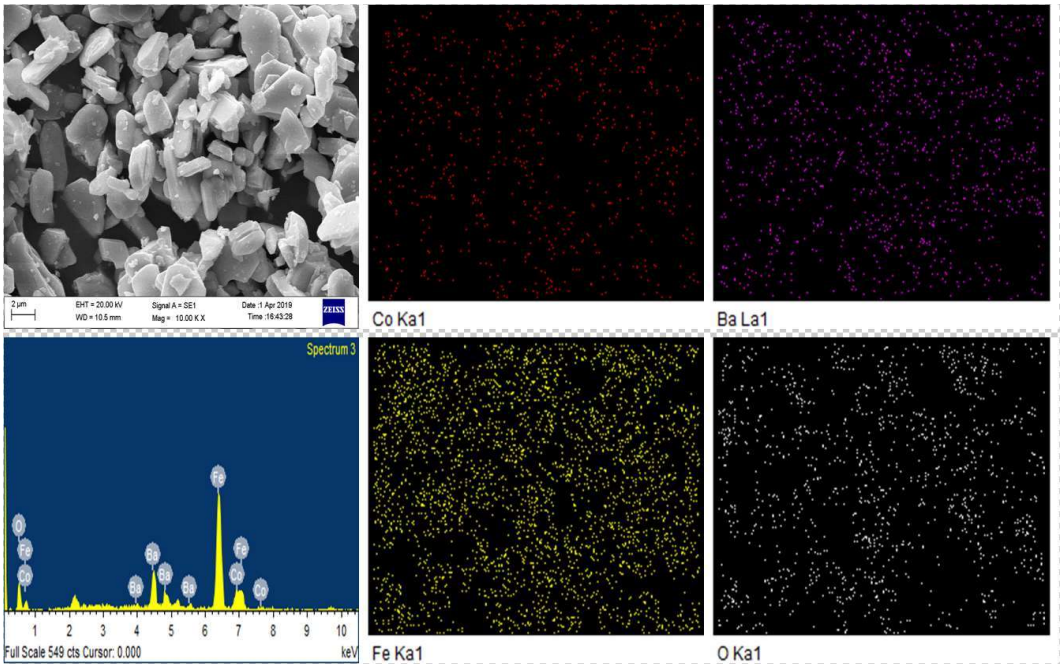

Figure 4.3 SEM, EDX, and Elemental mapping micrographs of calcined pure Y-type barium hexaferrite powder.

The microstructure of the calcined pure Y-type barium hexaferrite powder is shown in Fig. 4.3 along with EDX and elemental mapping micrograph. SEM micrograph of the calcined powder reveals that these particles are homogeneous with a nearly hexagonal plate-like shape in a range of 0.5 to 2.8 µm with an average size of 1.96 µm. To conclude the chemical composition and homogeneity of the sample, the EDX is performed, and the outcome of the EDX analysis appraises the atomic weight percentage of constituting cations in the samples. It is found that the percentage of cations is nearly accurate,

corresponding to the composition ratio of (1:1:6:11) in the desired formula. The elemental mapping micrographs of the ferrite show that Co, Ba, Fe, and O are distributed uniformly in the sample and confirm the purity of the sample.

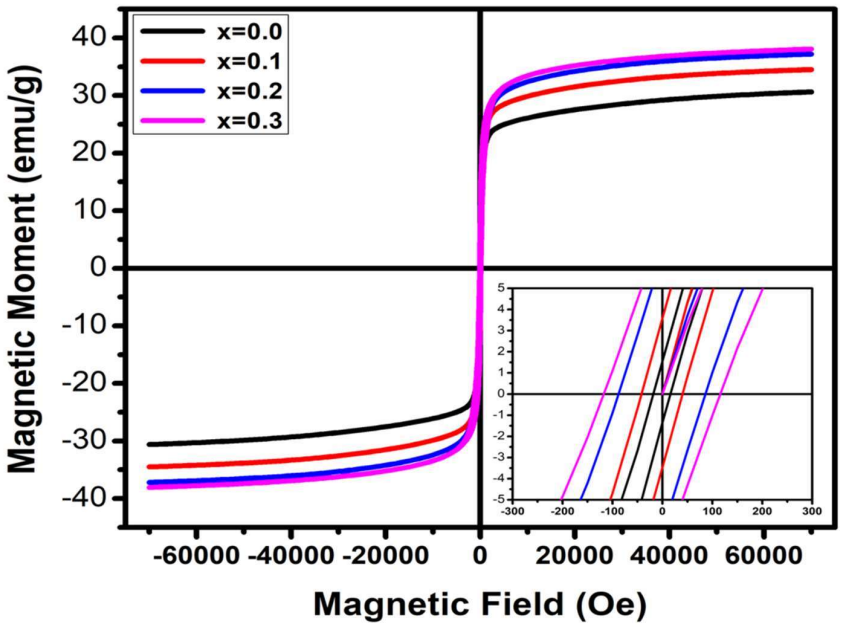

Figure 4.4 *M* versus *H* plot of calcined $Ba_{2-x}Ce_xCo_2Fe_{12}O_{22}$ (x = 0.0, 0.1, 0.2, & 0.3) ferrite powders at room temperature.

The small amount of Ce^{+3} ions substitution at the place of Ba^{+2} shows a significant impact on the magnetic properties in $Ba_2Co_2Fe_{12}O_{22}$ ferrite. Fig. 4.4 shows the magnetic hysteresis loops of $Ba_{2-x}Ce_xCo_2Fe_{12}O_{22}$ ferrite powders measured at 300 K under the maximum applied field of 70 kOe. The hysteresis loop (*M-H* curve) of all these powder samples shows ferrimagnetic behavior, and the magnetic parameters including Bohr magneton, saturation magnetization (M_s), remanent magnetization (M_r), squareness ratio (M_r/M_s), and coercivity field (H_c) are tabulated in Table 4.3.

As the cerium content increases, the value of Bohr magneton (N_{BM}) and saturation magnetization (M_s) increases continuously and reaches up to the value of 9.63 μB and 38.03 emu/g at x = 0.3. It can be interpreted based on the replacement of a magnetic ion Ce^{+3}

(having 1 μB magnetic moment) with a nonmagnetic Ba^{2+} ion [(Araz, 2019), (Mosleh *et al.*, 2016), (Abbas, Rao, *et al.*, 2014)]. The coercivity also follows the same increasing trend with $Ce^{3+,}$ and it is found to be the maximum value of 116.75 Oe, at x = 0.3. It may be explained by the existence of low spin Fe^{2+} ions along with high spin $Fe^{3+,}$ and it increases with cerium addition, resulting in greater coercive force [(C. J. Li *et al.*, 2012)]. The squareness ratio ($S_R = M_r/M_s$) is also an important characteristic parameter to determine the order of the magnetic hardness of any material. It shows a similar magnetic profile with soft ferrite (especially nickel ferrite nanoparticles *Ms* = 36.72 emu/g, *Hc* = 49.65 Oe); cerium substituted Y-type barium hexaferrite $Ba_{2-x}Ce_xCo_2Fe_{12}O_{22}$ may also be investigated in the oxidation of styrene [(Guin et al., 2005), (Singh & Sangwa, 2017)].

Table 4.3 Magnetic parameters N_{BM}, M_s, M_r, M_r/M_s, H_c of $Ba_{2-x}Ce_xCo_2Fe_{12}O_{22}$ (x = 0.0, 0.1, 0.2, & 0.3) ferrites.

Sample	N_{BM} (μB)	M_s (emu/g)	M_r (emu/g)	M_r/M_s	H_c (Oe)
$Ba_2Co_2Fe_{12}O_{22}$	7.74	30.58	1.55	0.051	16.97
$Ba_{1.9}Ce_{0.1}Co_2Fe_{12}O_{22}$	8.73	34.46	3.62	0.105	41.15
$Ba_{1.8}Ce_{0.2}Co_2Fe_{12}O_{22}$	9.42	37.16	6.62	0.178	86.92
$Ba_{1.7}Ce_{0.3}Co_2Fe_{12}O_{22}$	9.63	38.03	7.82	0.206	116.75

The reaction, which involves the oxidation of hydrocarbon to oxygenic compounds, is an essential part of the research in organic chemistry. Generally, the soft ferrites are identified as efficient oxidation catalysts and applied to transfer an oxygen atom from the oxidizing agent into hydrocarbon molecules present in the organic solvent [(Lindsay Smith *et al.*, 2006)]. Here, $Ba_2Co_2Fe_{12}O_{22,}$ synthesized by the sol-gel auto combustion method, is used as a catalyst to evaluate its catalytic efficiency. The oxidation reaction of styrene is used as a model reaction to evaluate its catalytic activity and results in to form of

benzaldehyde and other minor products [(Pawar & Pardeshi, 2014)]. It is the first attempt to use a hard magnetic ferrite as a catalyst in the oxidation of styrene as per Scheme 4.1.

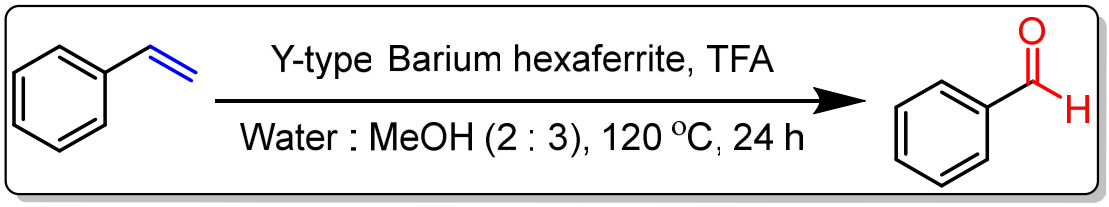

Scheme 4.1 Transformation of styrene to benzaldehyde in the catalytic presence of Y-type barium hexaferrite and TFA.

To confirm the need for the hexaferrite for selective oxidation of styrene, a blank reaction is conducted under similar conditions. As a result, there is no reaction takes place in the absence of the catalyst. To achieve the optimized conditions for this reaction, styrene is studied as a model substrate using TFA (trifluoroacetic acid) as an oxidant in the presence of various catalytic amounts of pure Y-type barium hexaferrite. According to Vishnetskaya *et al.*, TFA is found to be a promising oxidizing agent to activate the molecular oxygen dissolved in it, and it endows the acid with robust oxidizer properties [(Vishnetskaya et al., 2006)]. The amount of catalyst, reaction time, reaction temperature, and solvent are optimized for this model reaction. Due to the economic and environmental advantages, the mixture of water with methanol is selected as a solvent instead of other organic solvents like acetonitrile [(Nasseri *et al.*, 2014)], acetone [(Pawar & Pardeshi, 2014)], chloroform [(Kooti & Afshari, 2012)], 1,2-dichloroethane [(Kooti & Afshari, 2012)], 1,2-dichloromethane [(Nasseri *et al.*, 2014)], ethyl acetate [(Nasseri *et al.*, 2014)], etc.

Fig. 4.5 displays the influence of catalyst amount on the conversion and the selectivity of styrene after oxidation. It can be seen that initially, the conversion with lower addition (up to 5 mg) of barium hexaferrite is too less. Further increasing the amount of catalyst, the selectivity of benzaldehyde is increased. The increment in the catalyst amount

from 10 mg to 15 mg results in 88% improvement, and from 15 mg to 20 mg results in 40.42% improvement of yield for benzaldehyde selectivity in the final product. This may be due to the accessibility of a quite large surface area and more active sites, which help the scattering of species. With further increase up to 25 mg, it doesn't show further enhancement in the selectivity. It may be due to magnetic agglomeration that results in a lower contact area for reactants [(Tong, Li, Bo, Wang, Hu, Zhang, *et al.*, 2016)]. It may also be due to the adsorption of reactants on different catalyst particles, thus decreasing the chance of interrelating. The best selectivity of benzaldehyde is found at 20 mg of the catalyst with TFA as an oxidizing agent, and 20 mg is selected as the optimum catalyst amount for further processing.

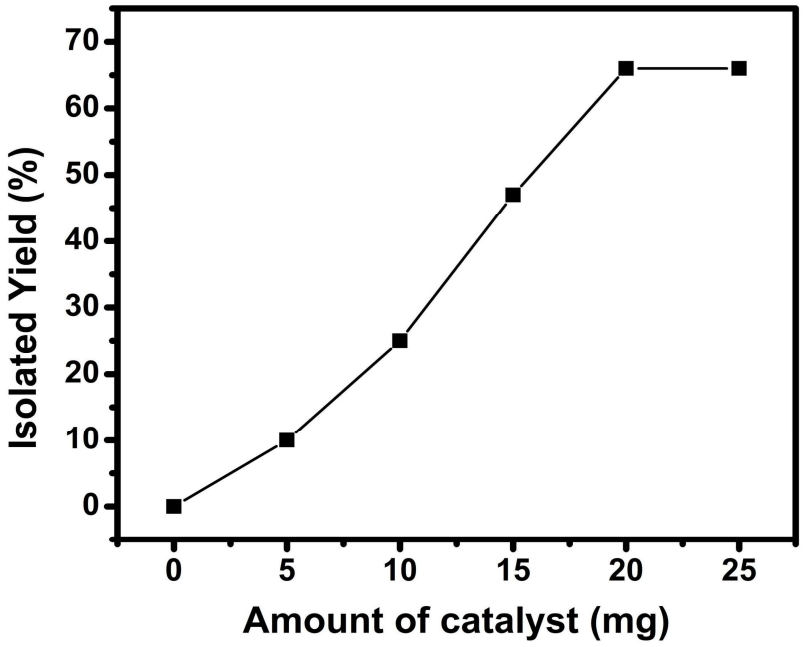

Figure 4.5 Influence of catalyst amount on the isolated yield for styrene in reaction product (Reaction conditions; Temperature 120°C, Time 24 hrs with TFA).

The impacts of reaction temperature on the styrene oxidation are estimated in the temperature range between 60 to 140˚C with the optimum catalyst amount (20 mg) and

TFA as an oxidizing agent for 24 hrs reaction. The result is shown in Fig. 4.6. It can be found that high temperature prefers both conversion and selectivity of benzaldehyde in the reaction product. It is revealed that the selectivity of benzaldehyde increases continuously with each step of 10˚C from 60 to 120˚C, respectively, and remains constant after that. This suggests that the bond C=C cleavage is more constructive with increasing temperatures. Above 120˚C, the increasing rate of selectivity becomes constant due to the faster evaporation rate of the solvent. Considering the energy balance, the best selectivity of benzaldehyde is found to be 66% at 120˚C with 20 mg of catalyst.

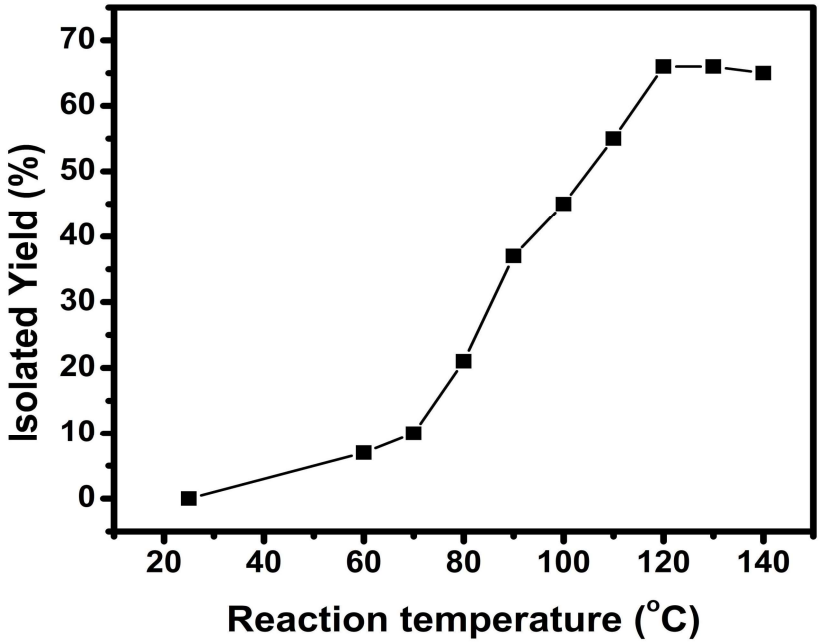

Figure 4.6 Influence of reaction temperature on the isolated yield for styrene in reaction product (Reaction conditions; Catalyst amount 20 mg, Time 24 hrs with TFA).

The effect of reaction time on the oxidation of styrene is inspected in the range of 2 to 26 hrs with the optimum amount of catalyst (20 mg) along with TFA as an oxidizing agent at 120˚C. Fig. 4.7 shows that the selectivity of the benzaldehyde is increased with the reaction time up to 24 hrs. After 24 hrs, the selectivity of the desired product becomes stable

at 66% due to the enhanced reaction time, which allows the formation of the byproducts. It may impede the further yield of the desired product due to the complete exhaustion of the oxidizing agent in the reaction mixture [(Pawar & Pardeshi, 2014)]. Taking energy into consideration, the 24 hrs reaction time is found appropriate for this reaction model with better efficiency for benzaldehyde production.

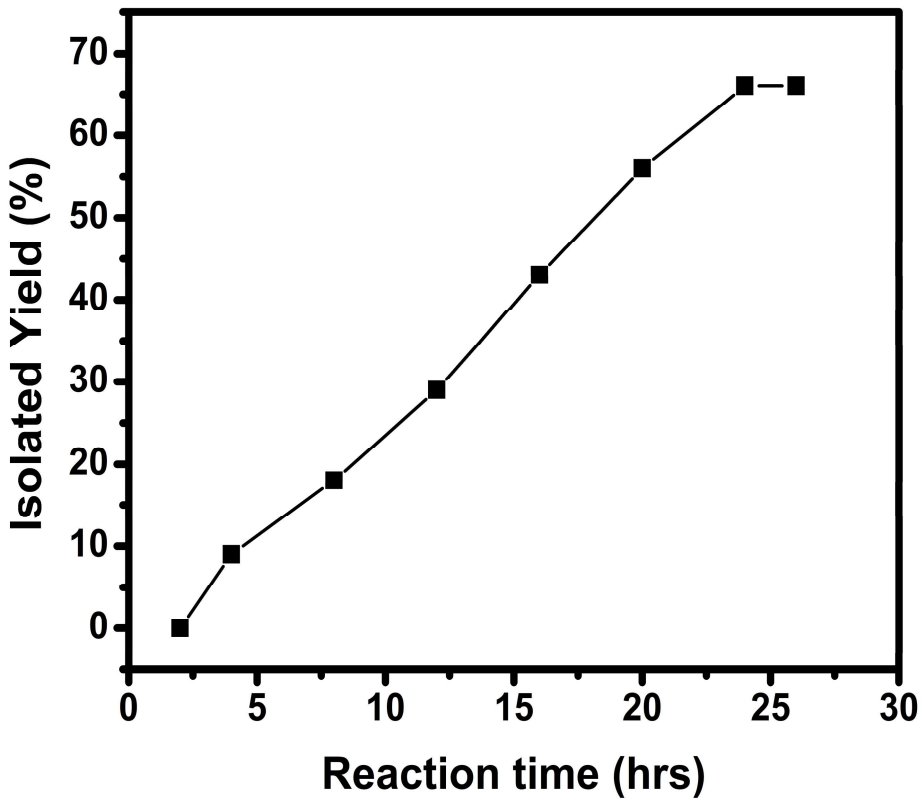

Figure 4.7 Influence of reaction time on the isolated yield for styrene in reaction product (Reaction conditions; Catalyst amount 20 mg, Temp. 120°C with TFA).

Table 4.4 shows the effect of the solvent (methanol to water ratio) on the selectivity of benzaldehyde in the model reaction. The water is not an organic solvent and shows less or nearly zero solubility compared with most organics. The optimization is done with the optimum amount of catalyst (20 mg) along with TFA as an oxidizing agent at 120˚C for 24 hrs reaction time.

Table 4.4 Influence of solvent on styrene oxidation.

S. No.	Solvent Ratio (MeOH: Water)	Catalyst	Cat. Amt. (mg)	Oxidizing agent	Temp. (˚C)	Time (hrs)	Yield (%)
1	0:1	Barium hexaferrite	20	TFA	120	24	Trace
2	1:0	Barium hexaferrite	20	TFA	120	24	32
3	1:1	Barium hexaferrite	20	TFA	120	24	16
4	2:1	Barium hexaferrite	20	TFA	120	24	46
5	3:2	Barium hexaferrite	20	TFA	120	24	66
6	1:2	Barium hexaferrite	20	TFA	120	24	Trace
7	2:3	Barium hexaferrite	20	TFA	120	24	12

Water (MW 18.015, density 1.00 g/mL, melting point 0°C, boiling point 100°C.) is considered a "polar protic solvent," which contains one or more hydrogen atoms that can be vanished as a proton in a transfer reaction. Mostly water is used with many polar organic co-solvents (methanol, ethanol, acetone, etc.) to enhance the solubility along with the properties of water itself [(Hultin, 2002)]. Initially, it depicts negligible selectivity for benzaldehyde. It may be due to the insolubility of styrene with water. Due to the environmental advantages of water compared with hazardous organic solvents, the water along with methanol (MW 32.042, density 0.791 g/mL, melting point –98°C, and boiling point 65°C) is selected as a co-solvent. The solvent (water) having a high dielectric constant helps styrene conversion, and the solvent (methanol) having a low dielectric constant helps the formation of benzaldehyde. Further, the addition of methanol results in increasing the

selectivity and yield up to 66% for benzaldehyde at 3:2 (MeOH: Water). Among various ratios of methanol and water, it is found that the optimized value of selectivity for benzaldehyde is obtained at MeOH: Water - 3:2 ratio.

Table 4.5 Influence of oxidizing agent on styrene oxidation.

S. No.	Catalyst	Cat. Amt. (mg)	Oxidizing agent	Temp. (˚C)	Time (hrs)	Yield (%)
1	Barium hexaferrite	20	PTSA	120	24	40
2	Barium hexaferrite	20	Pivalic acid	120	24	00
3	Barium hexaferrite	20	Terephthalic acid	120	24	Trace
4	Barium hexaferrite	20	TFA	120	24	66
5	Barium hexaferrite	20	HNO_3	120	24	00
6	Barium hexaferrite	20	H_3PO_4	120	24	Trace
7	Barium hexaferrite	20	H_2SO_4	120	24	00
8	Barium hexaferrite	20	Acetic acid	120	24	35

Table 4.5 shows the effect of various acids as an oxidizing agent for the selectivity of benzaldehyde in the oxidation of styrene with optimized reaction conditions. The selectivity of benzaldehyde with different oxidizing acids like p-toluene sulfonic acid (PTSA) [*(N. Li et al.*, 2015)], terephthalic acid [(N. Li *et al.*, 2015)], phosphoric acid [(Hultin, 2002)], pivalic acid [(Toledo *et al.*, 2012)], tri-fluoro acetic acid [(Kjonaas & Clemons, 2008)], nitric acid [(Anatoli Onopchenko Johann G. D. Schulz, 1975)], and acetic

acid [(Hirano *et al.*, 1980)] are analyzed. The best selectivity of benzaldehyde is found with TFA in optimized reaction conditions.

Table 4.6 Performance of as-prepared samples over the oxidation of styrene at optimized conditions.

S. No.	Catalyst	Cat. Amt. (mg)	Oxidizing agent	Temp. (˚C)	Time (hrs)	Yield (%)
1	$Ba_2Co_2Fe_{12}O_{22}$	20	TFA	120	24	66
2	$Ba_{1.9}Ce_{0.1}Co_2Fe_{12}O_{22}$	20	TFA	120	24	68
3	$Ba_{1.8}Ce_{0.2}Co_2Fe_{12}O_{22}$	20	TFA	120	24	71
4	$Ba_{1.7}Ce_{0.3}Co_2Fe_{12}O_{22}$	20	TFA	120	24	69

Table 4.6 displays the performance of the individual catalyst for benzaldehyde production through styrene oxidation within similar optimized conditions. As it is revealed that all these ferrite samples can proficiently catalyze the oxidation of styrene and benzaldehyde is confirmed as the foremost product in all cases. The results reveal that the Ce-substituted barium hexaferrite powders show higher performance than pure $Ba_2Co_2Fe_{12}O_{22}$ ferrite. The $Ba_{1.8}Ce_{0.2}Co_2Fe_{12}O_{22}$ composition shows the best performance within the model reaction with the highest yield (71%) for the desired product (benzaldehyde). Further increase in cerium content doesn't provide good selectivity due to the larger crystallite size (confirmed using XRD), resulting in a lower surface area as compared to the x = 0.2 sample. Hence, in the case of x = 0.3, a smaller number of active sites (surface oxygen vacancies) are available to provide oxidation of styrene, resulting in lower benzaldehyde selectivity.

XPS technique (from 1350 to 1 eV) is employed to examine the chemical composition of the surface elements in the as-prepared cerium substituted barium

hexaferrite ($Ba_{1.8}Ce_{0.2}Co_2Fe_{12}O_{22}$) sample, found best to achieve the highest selectivity for benzaldehyde.

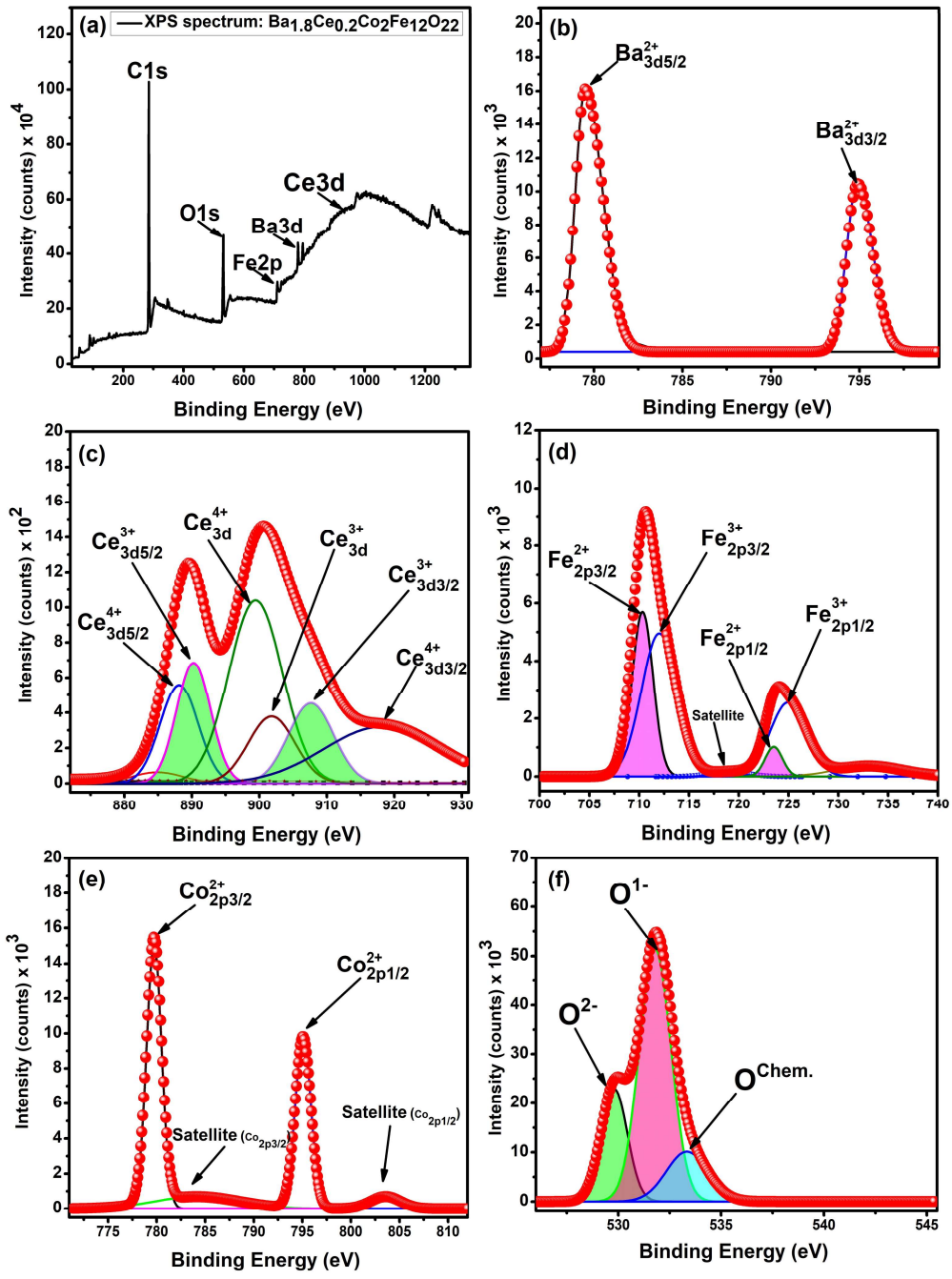

Figure 4.8 The XPS spectra of $Ba_{1.8}Ce_{0.2}Co_2Fe_{12}O_{22}$ surface (a) wide scan photoelectron spectra with high resolution spectrum corresponding to (b) Ba-3*d*, (c) Ce-3*d*, (d) Fe-2*p*, (e) Co-2*p*, (f) O-1*s* regions.

As demonstrated in wide scan XPS spectra (Fig. 4.8 (a)), the sample contains Ba, Ce, Fe, Co, and O elements, and no other contamination element is identified in the spectrum except carbon. The C1*s* peak is attuned to 284.8 eV and is considered as an internal standard for rectifying the binding energy for the other peaks [(Wu *et al.*, 2015)]. Fig. 4.8 (b) shows the high-resolution signal of Ba^{2+} 3*d* XPS spectra and confirms the presence of Ba^{2+} oxidation state by two broad peaks with corresponding binding energies of $Ba_{3d5/2}$ (779.5 eV) and $Ba_{3d3/2}$ (794.9 eV), respectively [(Ashraf *et al.*, 2020)]. Fig. 4.8 (c) illustrates a characteristic 3*d* spectrum of Ce^{3+} and Ce^{4+} ionic blend. Characteristic peaks of the Ce_{3d}^{4+} and Ce_{3d}^{3+} ion can be observed at 899.4 eV and 901.8 eV, respectively. Additionally, the peaks for $Ce_{3d5/2}^{4+}$ (884.9 eV), $Ce_{3d5/2}^{3+}$ (888.1 eV), $Ce_{3d3/2}^{3+}$(907.6 eV) and $Ce_{3d3/2}^{4+}$ (918.0 eV) have also been recognized within the sample [(Ahmad *et al.*, 2017), (Chen *et al.*, 2016)]. The analysis for the Co-2*p* spectrum in the sample becomes much more complicated due to the coexistence of the intensive Ba-3*d* spectrum within the same range of binding energies (780 to 795 eV). Fig. 4.8 (d) clarifies the presence of Co^{2+} with two symmetric peaks corresponding to the peak position for $Co_{2p3/2}^{2+}$ (779.7 eV) and $Co_{2p1/2}^{2+}$ (795.0 eV) spectrum associated with two satellite peaks at 782.2 and 803.8, respectively [(Fantauzzi *et al.*, 2019), (Zemek *et al.*, 1996)]. The incorporation of cerium in the sample leads to the coexistence of Fe^{2+} and Fe^{3+} oxidation states, which are confirmed by the Fe-2*p* spectra. As shown in Fig. 4.8 (e), two broad peaks associated with $Fe_{2p3/2}$ and $Fe_{2p1/2}$ peaks can be detected at 710.5 eV and 723.9 eV, along with two satellite peaks at 719.0 and 733.0 eV, respectively. These broad peaks for $Fe_{2p3/2}$ and $Fe_{2p1/2}$ are found to be a combination of two peaks in each at $Fe_{2p3/2}^{2+}$(710.3 eV), $Fe_{2p3/2}^{3+}$(712.0 eV), and $Fe_{2p1/2}^{2+}$(723.5 eV), $Fe_{2p1/2}^{3+}$(724.94 eV), respectively [(Zhou *et al.*, 2008), (Liu *et al.*, 2018)]. The high-resolution XPS spectrum for O1s confirms the presence of O2- oxidation state (Fig. 4.8 (f)) at the binding energy of 529.8 eV, native oxygen vacancy by the peak at

531.7eV and surface oxygen (due to the presence of H_2O or -CO_3 bonds on the surface) by the peak at 533.3 eV [(Lindsay Smith *et al.*, 2006), (Kjonaas & Clemons, 2008), (Anatoli Onopchenko Johann G. D. Schulz, 1975)]. The peak associated with oxygen vacancy agreed with the XRD results for $Ba_{1.8}Ce_{0.2}Co_2Fe_{12}O_{22}$, which shows that the addition of Ce ions results in the lattice contraction and generates oxygen vacancies. It can be concluded that the coexistence of Fe^{2+}, Fe^{3+}, and Ce^{3+}, Ce^{4+} ions in the sample causes the formation of oxygen vacancies with the substitution of Ce ions. The availability of surface oxygen vacancies is observed as the supreme reactive site in catalysis.

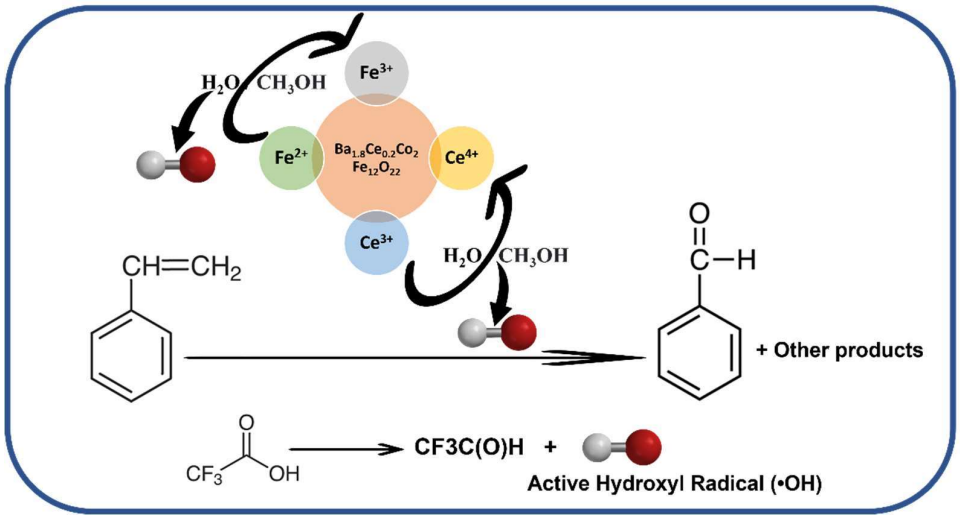

Figure 4.9 Plausible reaction mechanism for catalytic oxidation of styrene.

The promoting effect of the oxidation can be ascribed to the generation of active hydroxyl radicals (˙OH) by utilizing the existing redox configuration at the catalytic surface (both Ce^{3+}/Ce^{4+} & Fe^{2+}/Fe^{3+}) to disintegrate the solvent (water or methanol) molecules or by the dissociation of TFA molecules. The presence of oxygen vacancies over the catalytic surface may also facilitate the disintegration of water molecules into active hydroxyl radicals (˙OH), providing the opportunity to develop a vigorous catalyst in the presence of water vapor [(Younis *et al.*, 2018), (Kim *et al.*, 2015), (Tran *et al.*, 2019), (L. Li *et al.*,

2015)]. According to the proposed mechanism, initially, the styrene endures a C=C bond cleavage favorably over oxygen vacancy-rich hexaferrite surface to produce benzaldehyde as a major product along with a blend of several possible byproducts such as styrene oxide (by epoxidation), benzoic acid (by the deep oxidation of benzaldehyde), phenyl acetaldehyde (by the isomerization of styrene oxide). [(Pardeshi *et al.*, 2010), (Pardeshi *et al.*, 2011) (Belvedere *et al.*, 1983), (Liu *et al.*, 2022), (Francisco *et al.*, 1992), (Li, Z. *et al.*, 2012)]

The higher selectivity for benzaldehyde can be explained due to the presence of an oxygen vacancy cluster, which leads to a faster oxidation rate and doesn't allow further dissociation of the desired product. This increasing trend for benzaldehyde selectivity for $Ba_{1.8}Ce_{0.2}Co_2Fe_{12}O_{22}$ can also be linked to the presence of a well-known oxidation catalyst CeO_2 in the samples (as an impurity phase, confirmed by XRD). It provides easy coordination of organic ligands on Ce^{+3} active sites of CeO_2 [(Tong, Li, Bo, Wang, Hu, & Zhang, 2016)]. The lower value of selectivity and conversion in the case of $Ba_{1.7}Ce_{0.3}Co_2Fe_{12}O_{22}$ may be due to fewer oxygen vacancies in the active sites of the catalyst. Due to the highest benzaldehyde selectivity among all the prepared ferrite samples, the sample $Ba_{1.8}Ce_{0.2}Co_2Fe_{12}O_{22}$ is preferred as a catalyst to analyze further for its reproducibility and substrate scope.

After the optimization of reaction conditions in the model reaction, the catalyst $Ba_{1.8}Ce_{0.2}Co_2Fe_{12}O_{22}$ can be easily separated by the application of a magnetic field at the tube surface from the reaction mass. After separation, the same powder is used for the second run with the same optimized conditions. The selectivity of the benzaldehyde doesn't affect remarkably; a slight decrement is noticed, as shown in Fig. 4.9. It may be due to the inevitable losses associated with the separation process of catalyst. The optimization is done with the optimum amount of catalyst (20 mg) along with TFA as an oxidizing agent

and solvent (MeOH: Water - 3:2) at 120˚C for 24 hrs reaction time. So, the Ce-substituted barium hexaferrite can be considered a promising material in the selective oxidation of styrene, along with its better recyclability and benzaldehyde selectivity of approximately 71 %.

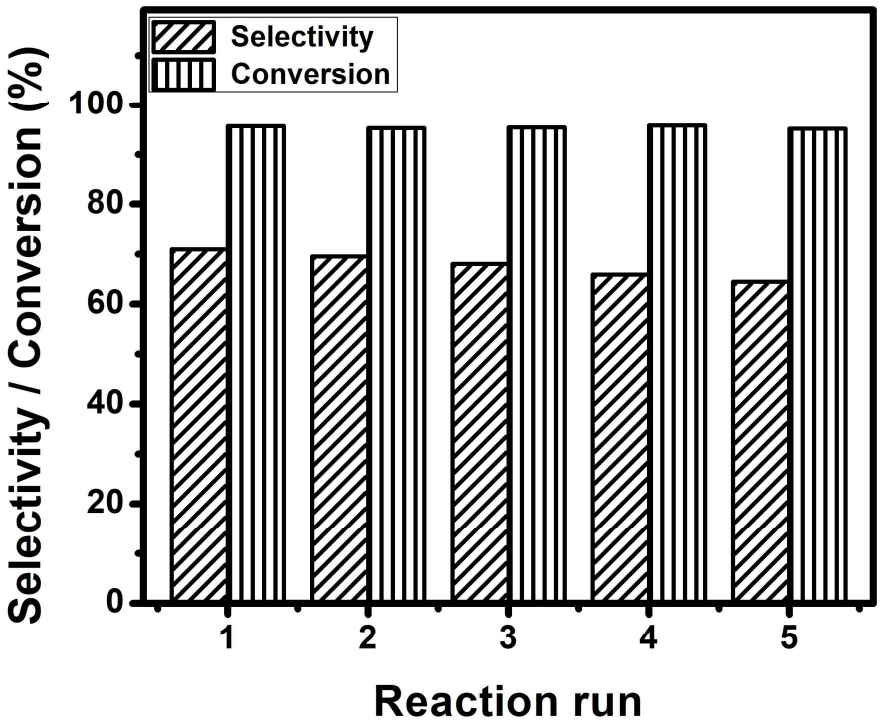

Figure 4.10 Reprocess of the catalyst $Ba_{1.8}Ce_{0.2}Co_2Fe_{12}O_{22}$ ferrite.

Table 4.7 displays the results of the selective oxidation of various substrates using $Ba_{1.8}Ce_{0.2}Co_2Fe_{12}O_{22}$ ferrite sample underneath with optimized conditions for the model reaction. It can successfully catalyze the oxidation of other cyclic olefins, likewise 4-methylstyrene, 4-chlorostyrene, 2,4-dimethylstyrene, 2-vinylnaphthalene, 4-methoxystyrene. Generally, it shows good selectivity of concerning products (more than 50% in all cases) and particularly shows 69% selectivity for 4-methylbenzaldehyde and 70% for 2-Naphthaldehyde. The reaction product, obtained in a solid/liquid state, is characterized by ^{1}H and ^{13}C NMR spectroscopy; the results confirm the presence of

constituting aldehyde by matching the standard peaks (shown in Table 4.8) for all these substrates.

Table 4.7 Substrates scope at optimized conditions for $Ba_{1.8}Ce_{0.2}Co_2Fe_{12}O_{22}$ ferrite.

S. No.	Reactant	Product	Benzaldehyde Yield (%)
1	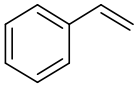	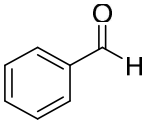	71
2	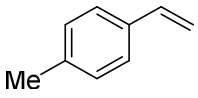	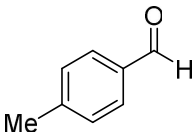	58
3	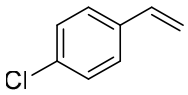	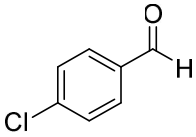	69
4	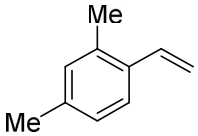	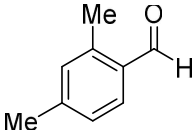	55
5	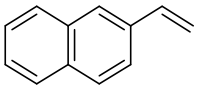	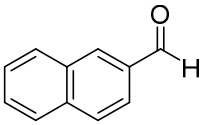	70
6	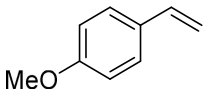	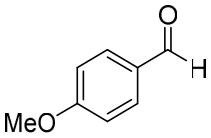	50

Table 4.8 Confirmation of reaction product obtained with various substrates using ^{1}H and ^{13}C NMR spectra.

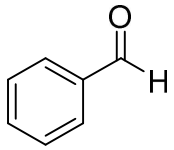	**Benzaldehyde**[1] **^{1}H NMR (400MHz, $CDCl_3$)**: δ = 10.00 (s, 1H), 7.64 – 7.88 (m, 2H), 7.60 – 7.64 (m, 1H), 7.50 – 7.60 (m, 2H). **^{13}C NMR (100MHz, $CDCl_3$)**: δ = 192.58, 136.45, 134.59, 129.85, 129.09.
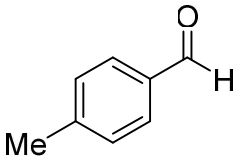	**4-MethylBenzaldehyde**[2] **^{1}H NMR (400MHz, $CDCl_3$)**: δ = 9.91 (s, 1H), 7.72 – 7.74 (m, 2H), 7.27 – 7.29 (m, 2H), 2.38 (s, 3H). **^{13}C NMR (100MHz, $CDCl_3$)**: δ = 192.18, 145.67, 134.22, 129.93, 129.79, 21.93.
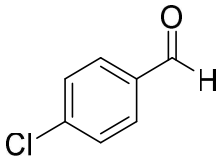	**4-ChloroBenzaldehyde**[3] **^{1}H NMR (400MHz, $CDCl_3$)**: δ = 9.97 (s, 1H), 7.83 – 7.79 (m, 2H), 7.51 – 7.48 (m, 2H). **^{13}C NMR (100MHz, $CDCl_3$)**: δ = 190.99, 141.05, 134.77, 131.00, 129.55.
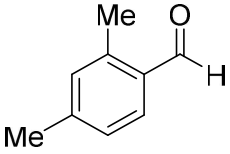	**2,4-dimethylbenzaldehyde** **^{1}H NMR (400MHz, $CDCl_3$)**: δ = 10.16 (s, 1H), 7.67 – 7.65 (m, 2H), 7.13 – 7.11 (m, 1H), 7.03 (s, 1H), 2.60 (s, 3H), 2.35 (s, 3H). **^{13}C NMR (100MHz, $CDCl_3$)**: δ = 192.53, 144.70, 140.70. 133.60, 132.50, 131.98, 127.16, 21.74, 19.63.
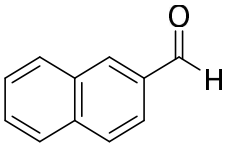	**2-Napthaldehyde**[1] **^{1}H NMR (400MHz, $CDCl_3$)**: δ = 10.15 (s, 1H), 8.33 (s, 1H), 8.01 - 7.66 (m, 4H), 7.66 – 7.25 (m, 2H), 7.50 – 7.60 (m, 2H). **^{13}C NMR (100MHz, $CDCl_3$)**: δ = 192.39, 136.54, 134.70, 134.18, 132.72, 129.62, 129.22, 129.20, 128.18, 127.19, 122.84.

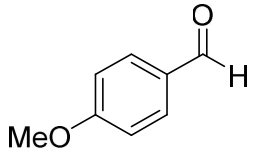	**2-Methoxybenzaldehyde**[1] **^{1}H NMR (400MHz, $CDCl_3$)**: δ = 9.81 (s, 1H), 7.78 – 7.76 (m, 2H), 6.94 – 6.92 (m, 2H), 3.81 (s, 3H). **^{13}C NMR (100MHz, $CDCl_3$)**: δ = 190.89, 164.66, 132.02, 129. 96, 114. 36, 55.62.

4.3 Summary

Cerium substituted nanocrystalline Y-type barium hexaferrite is successfully synthesized using sol-gel auto combustion with metal nitrates as precursors. This ferrite system can be selected as industrially adoptable catalysts for styrene oxidation reaction and the production of benzaldehyde. This work indicates that the catalytic activity of the complex ferrite is not only limited to conventionally use soft ferrites but also can be applied to some sort of hard ferrites. The as-prepared cerium substituted barium hexaferrite shows excellent catalytic performance because of its high surface area and large dispersity, which provides additional active sites for the reaction with trifluoroacetic acid (TFA) as an oxidant. A raise in styrene conversion is found with an increment in temperature. The optimum result shows that 20 mg of $Ba_{1.8}Ce_{0.2}Co_2Fe_{12}O_{22}$ ferrite displays a 71% yield for benzaldehyde at 120°C for 24 hrs. The higher selectivity for benzaldehyde can be explained due to the presence of an oxygen vacancy cluster. The catalyst is magnetically separable to reprocess. There is no remarkable loss of catalytic activity when it is reprocessed for five consecutive trials. It is concluded that the cerium substituted Y-type barium hexaferrite can also be used as a promising material in diverse oxidation reactions.